Author/s:
Huang, T;Holden, JA;Heath, DE;O'Brien-Simpson, NM;O'Connor, AJ

Title:
Engineering highly effective antimicrobial selenium nanoparticles through control of particle size

Date:
2019-08-21

Citation:
Huang, T., Holden, J. A., Heath, D. E., O'Brien-Simpson, N. M. & O'Connor, A. J. (2019). Engineering highly effective antimicrobial selenium nanoparticles through control of particle size. Nanoscale, 11 (31), pp.14937-14951. https://doi.org/10.1039/c9nr04424h.

Persistent Link:
https://hdl.handle.net/11343/339589

Nanoscale

Accepted Manuscript

This article can be cited before page numbers have been issued, to do this please use: T. Huang, J. Holden, D. E. Heath, N. O'Brien-Simpson and A. J. O'Connor, *Nanoscale*, 2019, DOI: 10.1039/C9NR04424H.

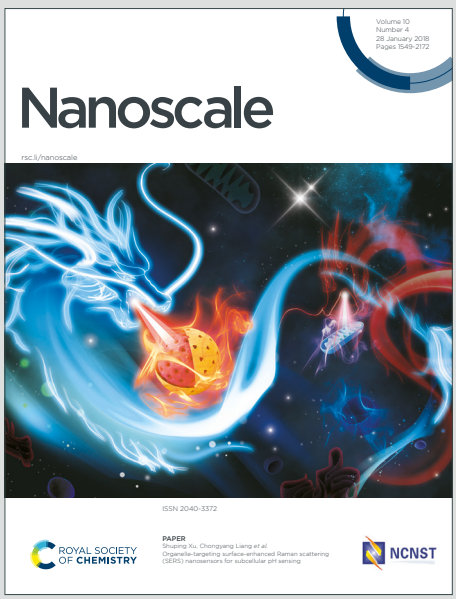

ROYAL SOCIETY OF CHEMISTRY

rsc.li/nanoscale

View Article Online
DOI: 10.1039/C9NR04424H

ARTICLE

Engineering highly effective antimicrobial selenium nanoparticles through control of particle size

Received 00th January 20xx,
Accepted 00th January 20xx

DOI: 10.1039/x0xx00000x

Tao Huang[a,b], James A. Holden[b], Daniel E. Heath[a], Neil M. O'Brien-Simpson[b], and Andrea J. O'Connor[a,*]

The overuse of antibiotics has induced the rapid development of antibiotic resistance in bacteria. As a result, antibiotic efficacy has become limited, and infection with multidrug-resistant bacteria is considered to be one of the largest global human health threats. Consequently, new, effective and safe antimicrobial agents need to be developed urgently. One promising candidate to address this requirement is selenium nanoparticles (Se NPs), which are made from the essential dietary trace element Se and have antimicrobial activity against Gram-positive bacteria. The size of nanomaterials can strongly affect their biophysical properties and functions; however, the effects of the size of Se NPs on their antibacterial efficacy has not been systematically investigated. Therefore, in this work, spherical Se nanoparticles (Se NPs) ranging from 43 to 205 nm in diameter were fabricated, and their mammalian cytotoxicity and antibacterial activity as a function of their size were systematically studied. The antibacterial activity of the Se NPs was shown to be strongly size dependent, with 81 nm Se NPs showing the maximal growth inhibition and killing of methicillin-sensitive and methicillin-resistant *Staphylococcus aureus* (MSSA and MRSA). The Se NPs were shown to have multi-modal mechanisms of action that depended on their size, including depleting internal ATP, inducing ROS production, and disrupting membrane potential. All the Se NPs were non-toxic towards mammalian cells up to 25 μg/mL. Furthermore, the MIC value for the 81 nm particles produced in this research is 16 ± 7 μg/mL, significantly lower than previously reported MIC values for Se NPs. This data illustrates that Se NP size is a facile yet critical and previously underappreciated parameter that can be tailored for maximal antimicrobial efficacy. We have identified that using Se NPs with a size of 81 nm and concentration of 10 μg/mL shows promise as a safe and efficient way to kill *S.aureus* without damaging mammalian cells.

Introduction

Infectious diseases cause 300 million cases of severe illness and about 16 million deaths every year [1]. The advent of antibiotics significantly reduced the morbidity and mortality caused by infections over the last century. However, the overuse of antibiotics induced the rapid development of microbial resistance to antibiotics and seriously limited the efficacy of current treatments. One approach to address this problem is developing new kinds of antibiotics. Unfortunately, the pipeline of antibiotic development is limited, and it is difficult to overtake the rapid evolution of antimicrobial resistance. Furthermore, conventional antimicrobial agents can lead to adverse side effects, particularly when increased doses are required to overcome the antibacterial resistance, leading to unacceptable toxicity for patients [2]. Therefore, alternative strategies to prevent and treat infections are urgently needed.

Because certain nanoparticles show good antibacterial activities and low toxicity towards mammalian cells [3, 4], antimicrobial nanoparticles are attracting increasing attention as a potential means to address this challenge. Compared to conventional antibiotics, antimicrobial nanoparticles have several potential advantages, including multiple modes of possible action on bacteria, simple and low-cost fabrication, and high stability. The ability to control infection with antimicrobial nanoparticles has been demonstrated *in vitro* and *in vivo* [5]. In addition, antimicrobial nanoparticles can damage bacteria through multiple pathways, making it more difficult for the bacteria to develop resistance [4, 6]. The enormous specific surface area and unique physical and chemical properties of antibacterial nanoparticles make them a promising next generation of antimicrobial agents [7].

Currently, silver nanoparticles (Ag NPs) are the most often used nanoparticles for antibacterial applications including the treatment of wound infections. Although Ag NPs have excellent antimicrobial activity, the toxicity of Ag NPs limits their applications. For example, Ag NPs exhibit cytotoxicity and genotoxicity to human cell lines [8, 9], induce changes in blood cell counts [10], prolonged exposure to soluble silver or uptake of high doses of silver can lead to an increase in inflammatory cytokines [11], and can induce irreversible pigmentation in the skin ('argyria') [12].

Se NPs have emerged as an attractive antimicrobial agent compared to Ag NPs. Unlike Ag, selenium is an essential trace element, a

[a] Department of Biomedical Engineering, Particulate Fluids Processing Centre, University of Melbourne, Parkville, VIC 3010, Australia.
E-mail: a.oconnor@unimelb.edu.au
[b] Melbourne Dental School and The Bio21 Institute of Molecular Science and Biotechnology, Centre for Oral Health Research, The University of Melbourne, Parkville, VIC 3010, Australia.
†Electronic Supplementary Information (ESI) available. See DOI: 10.1039/x0xx00000x

required cofactor for many proteins and enzymes in humans, and is also needed for proper muscular functions [13]. Selenium compounds have been widely explored due to their anticancer activities and low toxicity [14-16], and it has been observed that Se NPs exhibit lower cytotoxicity compared to selenium compounds [17]. Selenium is also an effective antioxidant, which can scavenge reactive oxygen species (ROS) in the body and protect cells from aging effects and apoptosis [18-21]. Se NPs were found to be absorbed and utilized more efficiently in the body than inorganic and organic selenium compounds when supplied via dietary intake [22-25].

The Se NPs can be produced through physical processes such as laser ablation [26, 27], chemical synthesis [28, 29], or biosynthesis [30, 31], and have antimicrobial activity. Se NPs have been shown to have antimicrobial activity against multiple types of Gram-positive bacteria [28, 30, 32], yet there is discrepancy in the literature over their ability to kill or inhibit Gram-negative bacteria [27, 28, 30]. For instance, Tran *et al.* found that selenium nanoparticles have effective antibacterial activity on *Staphylococcus aureus* (*S. aureus*) [28, 29] and that the ability to inhibit the growth of *S. aureus* began at low concentrations (1 μg/mL) [28]. The antibacterial effect of selenite and chitosan-modified selenium nanoparticles on *Lactobacillus bulgaricus* was also demonstrated [33]. Additionally, the antimicrobial activity of Se NPs is not limited to use in solution. Se NPs in composites or as material coatings have also exhibited good antibacterial activity [32, 34-37]. Biswas *et al.* compared the cytotoxicity and antibacterial activity of chitosan/PVA (polyvinyl alcohol) scaffolds loaded with either Ag NPs or Se NPs. The scaffolds decorated with Se NPs exhibited antibacterial activity towards *S. aureus*, *Escherichia coli* (*E. coli*) and methicillin-resistant *S. aureus* (MRSA) and were also much more cytocompatible with fibroblasts than the Ag NPs decorated scaffolds [32]. Furthermore, Se NPs have also been shown to possess the ability to kill bacteria in a biofilm and even destroy microbial biofilms *in vitro* at high doses (60 μg/mL)[38].

In addition to possessing antimicrobial activity towards bacteria, the Se NPs also exhibit antifungal properties. Yip *et al.* found that fabrics treated with Se NPs modified with a polysaccharide-protein complexes isolated from mushrooms could inhibit the growth of *Trichopyton rubrum* by more than 99.7% over 7 days [39]. Additionally, Ismial *et al.* assessed the *in vitro* antifungal effect of Se NPs on *Alternaria solani*, a pathogenic fungus that causes early blight disease of potatoes, and illustrated that a concentration of 800 μg/mL of Se NPs was sufficient to completely inhibit *A. solani* [40]. Additionally, Guisbiers *et al.* found that Se NPs fabricated by femtosecond pulsed laser ablation could inhibit *Candida albicans* biofilm formation [41].

Although, there are multiple studies investigating the antimicrobial activity of Se NPs, the results reported in the literature are variable. We hypothesise that these divergent results arise from different particle properties, preparation methods, and antimicrobial assays. It is well documented that the size, shape and surface chemistry of NPs can significantly affect their cellular interactions [42-45]. Despite this knowledge, the influence of size on the cytotoxicity and antibacterial activity of Se NPs has not been systemically investigated. In this study, spherical Se NPs ranging in size from ~40 to 200 nm were produced with a consistent capping agent (polyvinyl alcohol) and their antibacterial activity and cytotoxicity as a function of size and concentration were investigated. We identified that nanoparticle size is a key parameter that can be engineered to drastically improve the antimicrobial activity of the Se NPs while maintaining a high degree of cytocompatibility. These results identify a facile, yet previously unidentified method, of regulating Se NP bioactivity and provide a path forward for designing Se NP-based treatments with higher efficacy.

Results

Synthesis and characterisation of selenium nanoparticles with well controlled sizes

The synthesis conditions, mean sizes, and zeta potentials of the Se NPs are shown in Table S1. The reaction system used in this work was able to produce Se NPs with a minimum diameter of ~40 nm. As such, the synthesis and characterisation of Se NPs with mean sizes ranging from ~40 – 200 nm are reported in this contribution. The size distributions of the Se NPs (Fig. S1) are monomodal and reasonably narrow, with polydispersity indices (PDI) of less than 0.1. There is no significant difference between zeta potentials of the different sized Se NPs, with average zeta potentials of approximately -5 mV. It has been reported previously that PVA capped nanoparticles showed zeta potentials of -10 to +10 mV [46, 47]. These nanoparticles form stable suspensions, mainly due to the steric stabilization of PVA instead of purely electrostatic stabilization [47]. With increasing nanoparticle size, the colours of the suspensions change from light yellow to light orange, and then to pink (Fig. S2). It has been reported previously that selenium nanoparticles suspensions are red in colour [48]. At higher concentrations the colour of the smaller sized Se NPs changed to dark orange or red, but the 205 nm Se NPs retain their pink colour. These results illustrate that the colour of a Se NP suspension is both size and concentration dependant.

Transmission electron microscopy (TEM) images of different sizes of Se NPs are shown in Fig. 1 (a)-(e). The nanoparticles are spherical and monodisperse, indicating that PVA is a good stabilizer. The TEM diffraction pattern of Se NPs shows diffuse rings (Fig. 1(f)), indicating that these Se NPs are amorphous. The nanoparticles are mainly composed of selenium according to energy dispersive spectroscopy (EDS) (Fig. 1(g)). Other peaks were attributed to the TEM mesh support (Cu, C) and the PVA (C, O).

FT-IR was used to investigate the interaction between the Se NPs and the PVA, shown in Fig. 1(h). For the pure PVA, the peak at 3307 cm^{-1} corresponded to O-H stretching vibrations. The peaks at 2914 cm^{-1} and 2943 cm^{-1} corresponded to C-H stretching from the alkyl group. The peaks lower than 2500 cm^{-1} were at 1732 cm^{-1} (C=O stretching), 1435 cm^{-1} (C-H bonding), 1261 cm^{-1} (C-O starching), 1100-1000 cm^{-1} (C-O stretching in C-O-H groups and COC groups), 849 cm^{-1} (C-H rocking mode), and 650 cm^{-1} and 570 cm^{-1} (out–of–plane vibration of C-H groups) [49, 50]. The peak at 1140 cm^{-1} was related to the crystalline C-O stretching vibration of PVA [49]. Compared to the spectrum of pure PVA, the PVA on the surface of Se NPs showed a shift in the hydroxyl peak to 3350 cm^{-1}. This blue-shift indicated that PVA was conjugated to the surface of Se NPs through the –OH group [51]. Further, the appearance of a new peak at 1649 cm^{-1} also indicated interactions between the C=O group of the PVA and the Se NPs [52].

81 nm Se NPs were the most effective at inhibiting the growth of S. aureus and MRSA

The growth curves of *S. aureus* in Mueller Hinton Broth (MHB) incubated with different weight concentrations and sizes of Se NPs

View Article Online
DOI: 10.1039/C9NR04424H

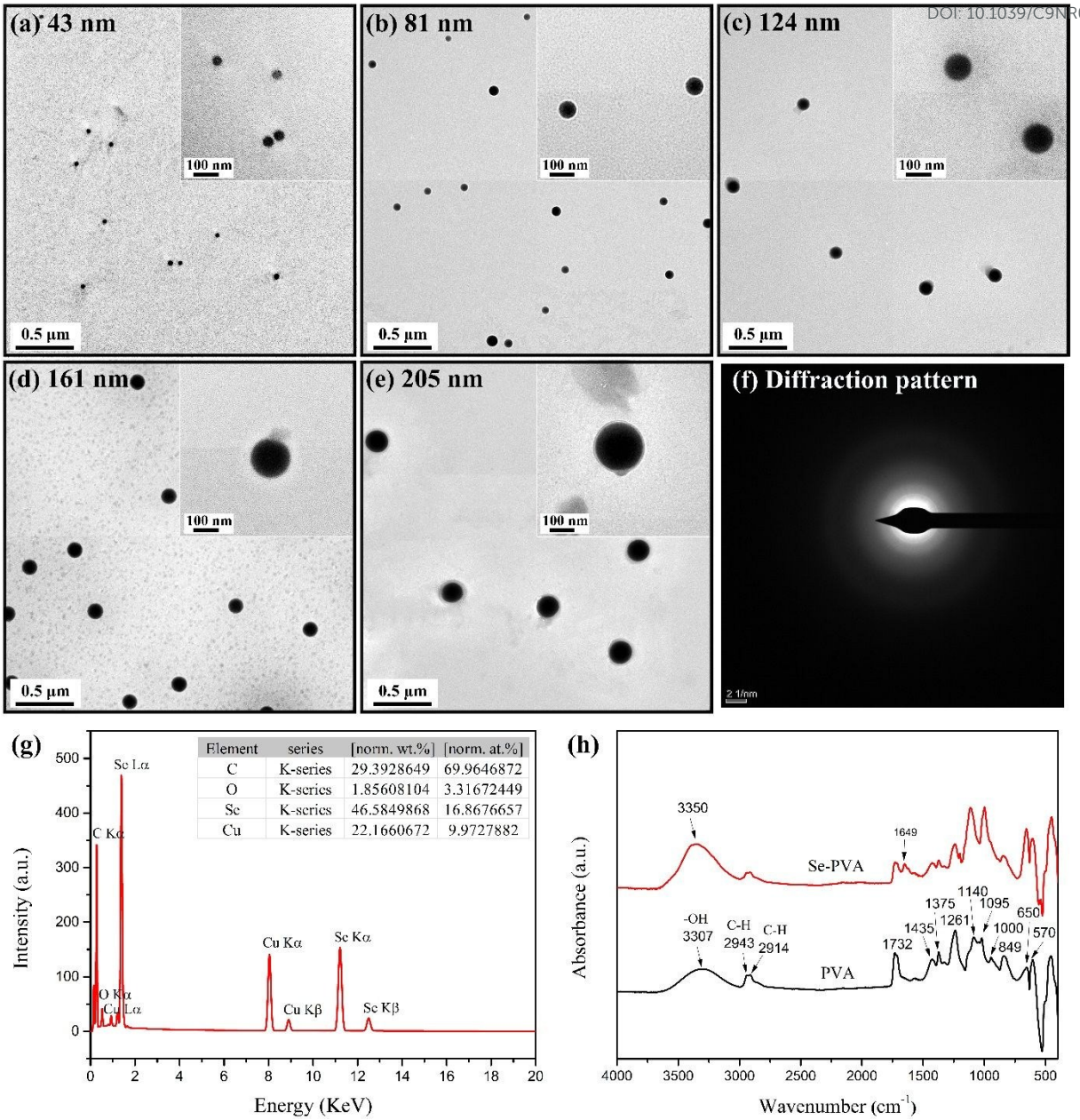

Fig. 1 TEM images of Se NPs with different mean sizes, as determined by dynamic light scattering: (a) 43 nm, (b) 81 nm, (c) 124 nm, (d) 161 nm and (e) 205 nm. (f) The TEM diffraction pattern, (g) the EDS spectra, and (h) the FT-IR spectra of the 81 nm Se NPs (red curve) and of pure PVA (black curve).

were measured (Fig. 2). The 81 nm Se NPs were the most effective at inhibiting the growth of *S. aureus*. This inhibition is dose dependent, starts from a very low Se NP concentration (0.78 μg/mL), and increases markedly with concentration. The other sizes of Se NPs also show inhibition effects that tend to increase with Se NP concentration but are much weaker than those for the 81 nm Se NPs. The minimum inhibitory concentrations (MIC) of the different Se NPs on *S. aureus* were calculated based on the growth curves and are listed in Table 1. The MIC values corroborate that the 81 nm particles were the most effective at inhibiting the bacterial growth (with $p < 0.05$).

To investigate whether nanoparticle size or nanoparticle number plays the dominant role in their antibacterial activity, the effects of Se NPs on *S. aureus* cultures were also assessed as a function of number concentration (Fig. 3). The conversion between number and weight concentration for Se NPs is compiled in Table S2. The 81 nm Se NPs were also found to be the most effective in inhibiting *S. aureus* growth as a function of number concentration (Fig. 3). At number concentration of 2.56×10^{10} particles/mL, the 124 nm (140 μg/mL) were at a much higher weight concentration than the 81 nm Se NPs (25 μg/mL). However, despite the much higher dose, the antimicrobial efficacy of 124 nm NPs was inferior to that of 81 nm NPs. These results indicated that the size of these Se NPs plays the dominant role in determining the antibacterial activity.

View Article Online
DOI: 10.1039/C9NR04424H

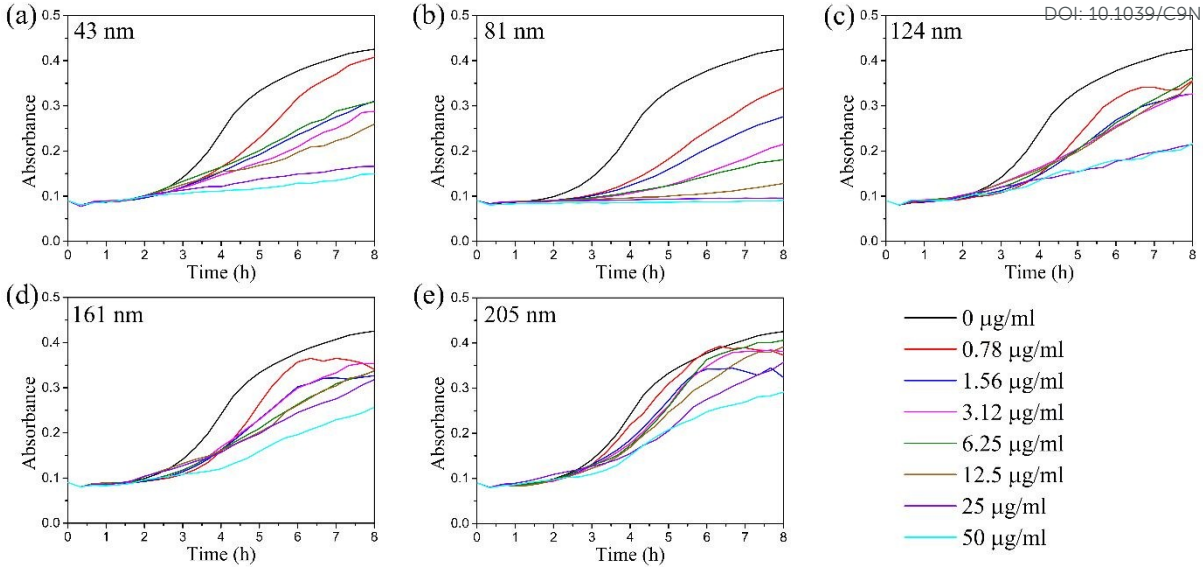

Fig. 2 Growth curves of *S. aureus* in MHB with different weight concentrations and sizes of Se NPs.

Table 1 The MIC and MBC values of Se NPs with different sizes on *S. aureus* and MRSA

Materials		Different sizes of Se NPs (nm)					Antibiotics	
		43	81	124	161	205	Methicillin	Vancomycin
S. aureus	MIC (μg/mL)	66 ± 13†	16 ± 7	85 ± 2†	100 ± 15†	123 ± 34†	1.56	0.78
	MBC (μg/mL)	97 ± 35†	35 ± 16	147 ± 38†	156 ± 30†	257 ± 68†	/	/
MRSA	MIC (μg/mL)	29 ± 1	12 ± 2	46 ± 4	73 ± 7†	107 ± 21†	>128	1.56
	MBC (μg/mL)	59 ± 11†	18 ± 7	114 ± 46†	158 ± 25†	199 ± 7†	/	/

* The data of Se NPs are expressed as mean± standard deviation (s.d.) of the biological replicates. † As these sizes of Se NPs showed no total inhibition of growth or killing of bacteria within the tested concentrations, these MIC and MBC values, calculated through linear fitting, are only for comparison. MIC for methicillin and vancomycin are included to validate the antibiotic sensitivity and resistance of the *S. aureus* strains.

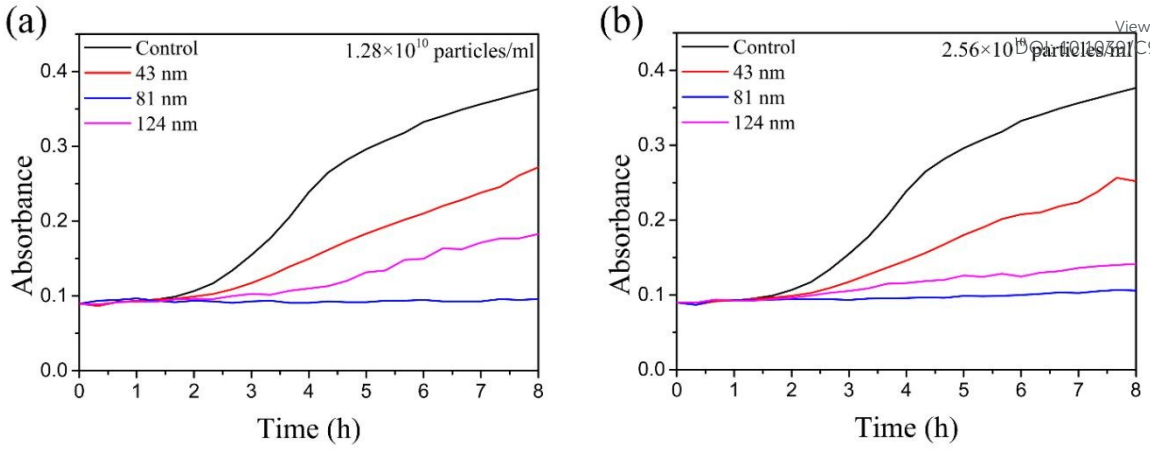

Fig. 3 Growth curves of *S. aureus* in MHB with different number concentrations and sizes of Se NPs.

As Se NPs were effective against antibiotic-sensitive *S. aureus,* their effect on the growth of MRSA was determined (Fig. 4). The 81 nm Se NPs were found to be the most effective at inhibiting the growth of MRSA. Interestingly, according to the MIC values (Table 1), the 43 nm, 124 nm and 161 nm Se NPs were more effective at inhibiting the growth of MRSA compared to the results with antibiotic-sensitive *S. aureus*. This indicates that MRSA is more sensitive to these Se NPs than antibiotic-sensitive *S. aureus*.

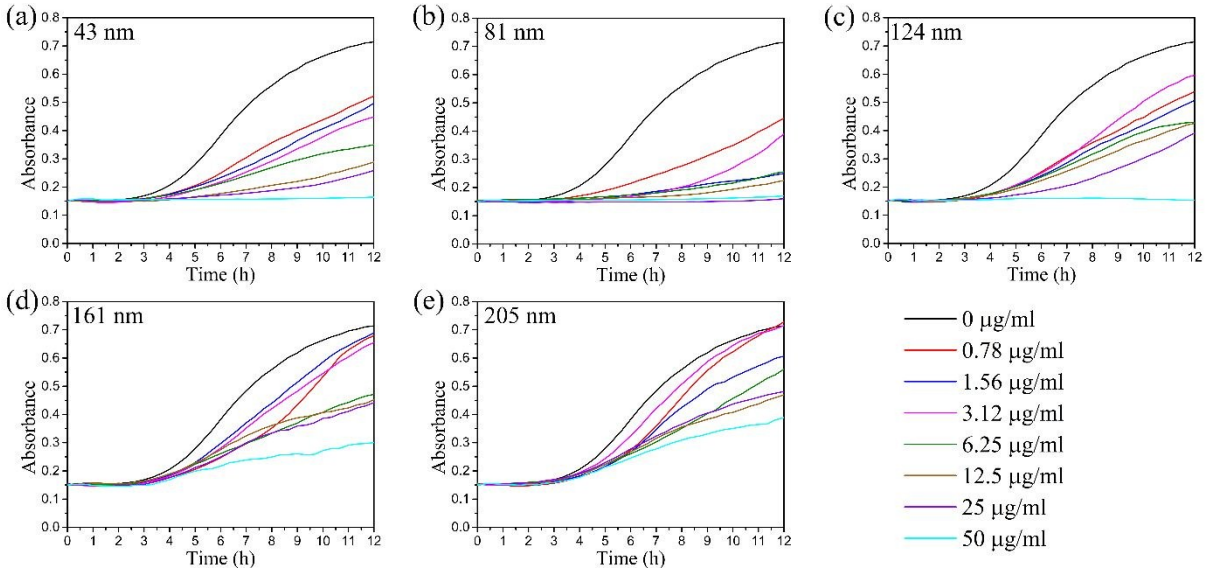

Fig. 4 Growth curves of MRSA in MHB with different weight concentrations and different sizes of Se NPs.

The colony forming unit (CFU) assay was used to assess the ability of Se NPs to kill *S. aureus* and MRSA (Fig. 5), and the minimum bactericidal concentrations (MBC) were calculated from the CFU data (Table 1). The results from the CFU assay support the results of the bacterial growth inhibition tests, with the 81 nm Se NPs showing the greatest antimicrobial activity. At concentrations ≤ 50 μg/mL, only the 43 nm and 81 nm Se NPs showed significant bactericidal activity towards *S. aureus* (Fig. 5 (a)). However, the minimum concentration at which the 81nm Se NPs showed a significant bactericidal effect (0.78 μg/mL) is significantly ($p < 0.05$) lower than that for the 43 nm particles (12.5 μg/mL). Interestingly, all sizes of Se NPs showed antibacterial activity towards MRSA at concentrations greater than or equal to 25 μg/mL (as shown in Fig. 5 (b)). These results indicate again that MRSA is more susceptible to the antimicrobial activity of the Se NPs than the antibiotic-sensitive *S. aureus*. The 81 nm Se NPs had the greatest bactericidal effect and at significantly lower concentrations than the other Se NPs.

The Se NPs have many potential mechanisms of action

Four different mechanisms of action were investigated that may lead to the observed antimicrobial properties of the Se NPs: (1) metabolic interference through disruption of intercellular adenosine triphosphate (ATP) concentrations, (2) modulation of the intracellular concentration of reactive oxygen species (ROS), (3)

depolarisation of the bacterial membrane, and (4) disruption of the bacterial membrane. ATP is the intracellular energy used by all living organisms. It plays a vital role in both respiration and metabolism as it is the most important energy supplier for many enzymatic reactions [53]. We therefore investigated the effects of different concentrations and sizes of Se NPs on the ATP level of *S. aureus*. *S. aureus* cultures treated with Se NPs showed a significant decrease in ATP, with the 81 nm particles inducing the greatest depletion (Fig. 6(a)). This fast depletion of cellular ATP is a characteristic of an energy-uncoupling effect [54].

The oxidative stress induced by high ROS production in response to nanoparticles is another mechanism that can lead to bacterial death [55]. Therefore, we investigated the effect of different concentrations and sizes of Se NPs on ROS production (Fig. 6(b)). Se NPs promoted ROS production in *S. aureus* cells, with both 43 nm and 81 nm Se NPs resulting in a statistically significant increase in ROS as compared to the control without particles.

Depolarisation of cell membranes is a well-established mechanism of action of antimicrobial agents [56]. Therefore, we also investigated the effects of Se NPs on the polarity of the *S. aureus* cell membranes (Fig. 6(c)). *S. aureus* treated with 43 nm and 81 nm Se NPs led to mild depolarization of the membrane in a dose dependent manner.

Helium Ion Microscopy (HIM) was used to observe *S. aureus* cells after treatment with different sizes of Se NPs (Fig. 6(d-k)). The low magnification images (Fig. 6(d-g)) allow the visualisation of cellular morphology, while the higher magnification images (Fig. 6(h-k)) reveal details about the topography of the bacterial cell walls. The untreated *S. aureus* cells were spherical, and their surfaces were smooth. In contrast, the majority of *S. aureus* cells treated with 43 nm Se NPs exhibited a rough/wrinkled cell wall topography and some had ruptured membranes. Most of the *S. aureus* cells treated with the 81 nm Se NPs had wrinkled cell wall topography compared to the control; however, minimal cell wall disruption was observed. The cells treated with the larger 124 nm particles largely retained their spherical shape and smooth cell wall. The higher magnification images also enable the visualization of some Se NPs that have attached to the cell wall.

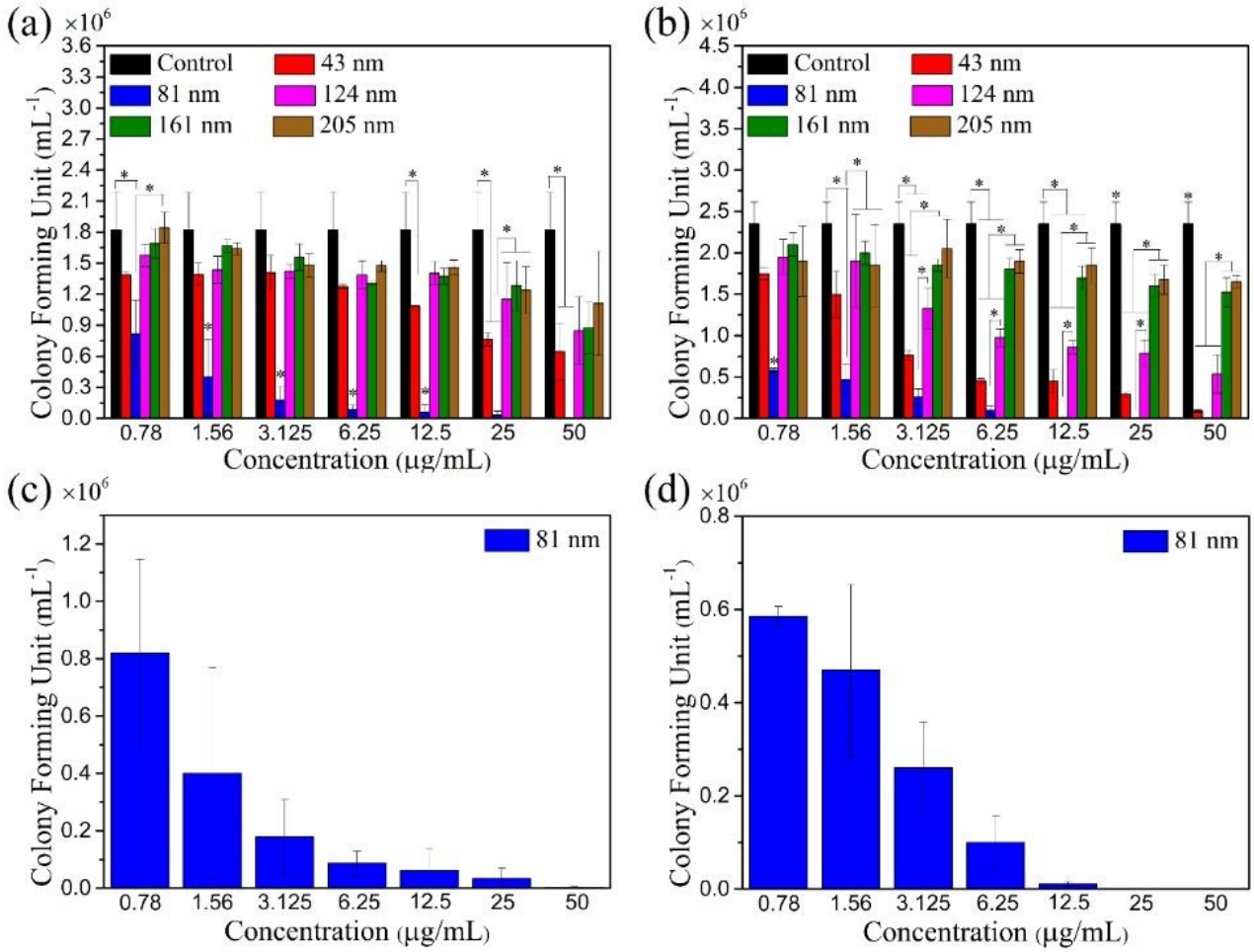

Fig. 5 Colony forming units assay results for (a) *S. aureus* and (b) MRSA in MHB with different concentrations and sizes of Se NPs. A One-Way ANOVA followed by a Tukey's Post Hoc Test was used to compare the means, Asterisks denote significant difference, * p-value < 0.05. (c) and (d) show the CFU results magnified for 81 nm on *S. aureus* and MRSA, respectively.

View Article Online
DOI: 10.1039/C9NR04424H

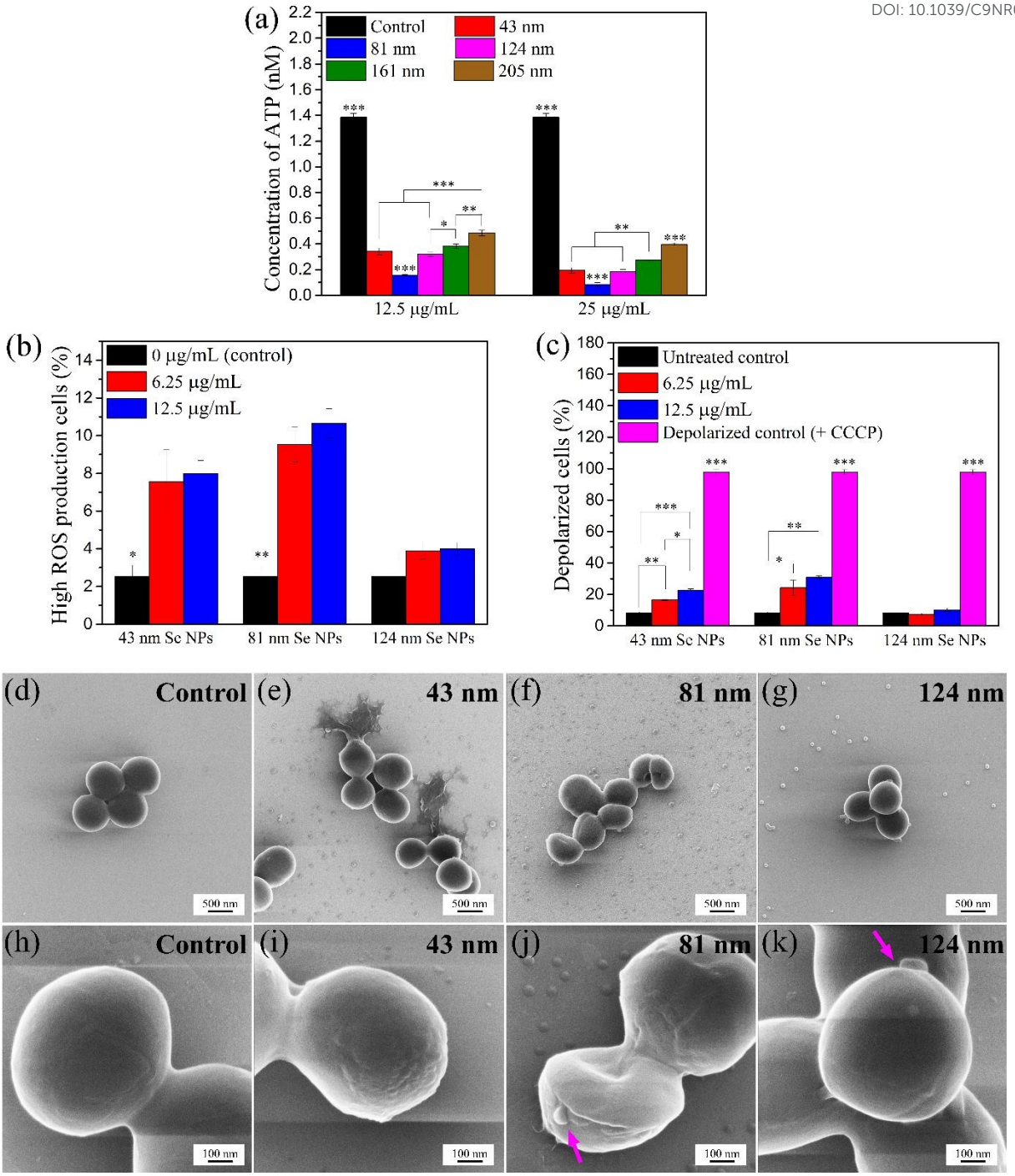

Fig. 6 (a) ATP level of *S. aureus* with different sizes of Se NPs, with bacteria in pure MHB as a control, (b) the percentage of *S. aureus* cells with high ROS production after treatment with different sizes of Se NPs, with bacteria in pure MHB as a control and (c) the percentage of depolarized *S. aureus* cells after treatment with different sizes of Se NPs. One-way ANOVA was used to compare means of experimental groups, * p-value < 0.05, ** p-value < 0.01 and *** p-value < 0.001. The asterisk(s) directly marked on a bar indicate(s) this group is significantly different to all other groups. (d)-(k) are helium ion microscopy images of *S. aureus* with different sizes of Se nanoparticles, with *S. aureus* in pure MHB as a control. The arrows point to Se NPs that are attached to the bacterial membrane.

Selenium nanoparticles do not exhibit cytotoxicity towards human dermal fibroblasts

The cytotoxicity of the Se NPs towards human dermal fibroblasts was assessed using the Cell Counting Kit-8 cell viability assay (CCK-8 assay). The viabilities of human dermal fibroblasts (HDFs) exposed to different concentrations and sizes of Se NPs for 24 h are shown in Fig. 7. HDFs exposed to Se NP concentrations up to and including 10 μg/mL showed viabilities statistically equal to – or greater than – the untreated control. The viability of HDFs exposed to the highest dose of 25 μg/mL of the 43 and 81 nm particles was ~80%, while the

View Article Online
DOI: 10.1039/C9NR04434H

viabilities for the cells exposed to the larger particles was ~100%. International Standard ISO 10993-5 describes assessment of *in vitro* cytotoxicity and states that reductions in viability of < 30% are not considered as toxic effects [57]. As such, none of the treatments, regardless of particle size or concentration, are classified as cytotoxic after 24 h of exposure.

Two assays were performed to further assess the interactions of the Se NPs with the mammalian cells. First, a lactase dehydrogenase (LDH) assay was used. This assay measures the amount of LDH present in the culture medium. As this enzyme is present within the mitochondria of living cells, increased levels of the LDH in the culture medium imply rupture of the cell membranes. Second, it has been shown that Se NPs can impact the production of reactive oxygen species (ROS) of mammalian cells [20, 58], and the levels of ROS impact cell viability. As such, a ROS production assay was also used.

The results of the LDH assay (Fig. S3) indicate treatment with Se NPs with concentrations up to 50 µg/mL does not induce obvious damage to the cell membranes of the HDFs over a 6 h period. The ROS production of HDFs upon exposure to Se NPs was also assessed (Fig. 8). Previous research has illustrated that low levels of selenium help cells clear ROS while higher doses will catalyse the production of ROS [59]. For instance, Chen *et al.* reported that the production of ROS induced by Se NPs was an important factor in causing cell apoptosis [60]. For the majority of the treatments, our data reveals no statistical differences in ROS production. However, a decrease in ROS production was observed for cells treated with 2.5 and 5 µg/mL of the 43 nm Se NPs. This decrease in ROS could partially explain the increased viability of the HDFs in response to the lower doses of the 43 nm particles (Fig. 7). However, no statistically significant reduction in ROS is observed for treatments with the 81 nm particles, while an increase in viability for some of these treatments was observed. This data implies that either 1) another mechanism is at least partially responsible for the increased viability of cells treated with the 81 nm particles, or 2) the ROS assay was not sensitive enough to reveal the variations in the ROS production in this system.

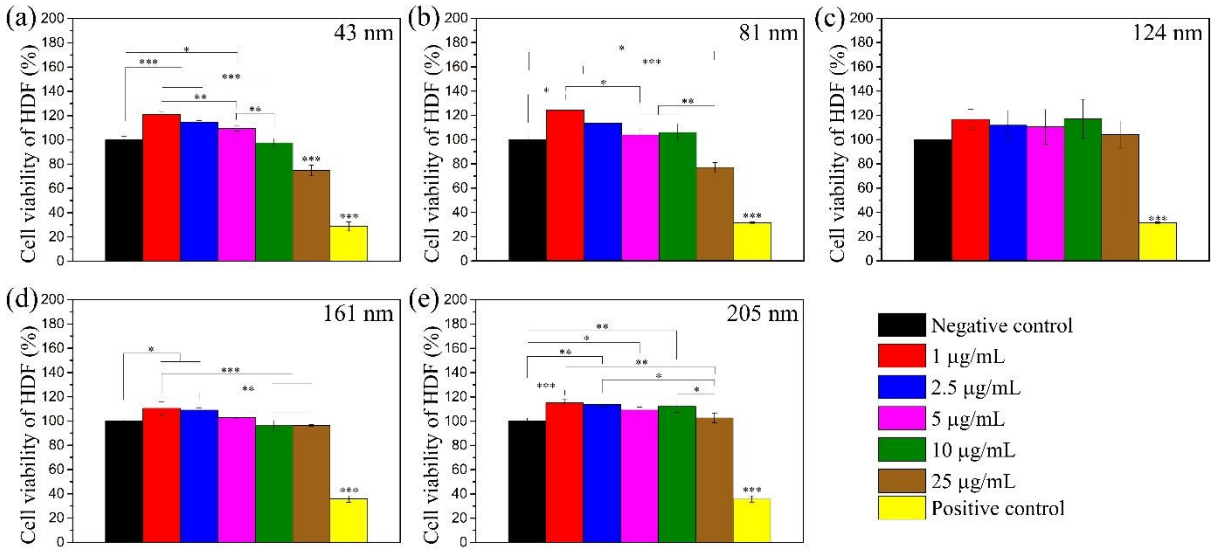

Fig. 7 Viability of human dermal fibroblasts after 24 h of treatment with different concentrations and sizes of Se NPs. A One-Way ANOVA followed by a Tukey's Post Hoc Test was used to compare means of all treatments. Asterisks denote the level of significance: * p-value < 0.05, ** p-value < 0.01 and *** p-value < 0.001.

View Article Online
DOI: 10.1039/C9NR04424H

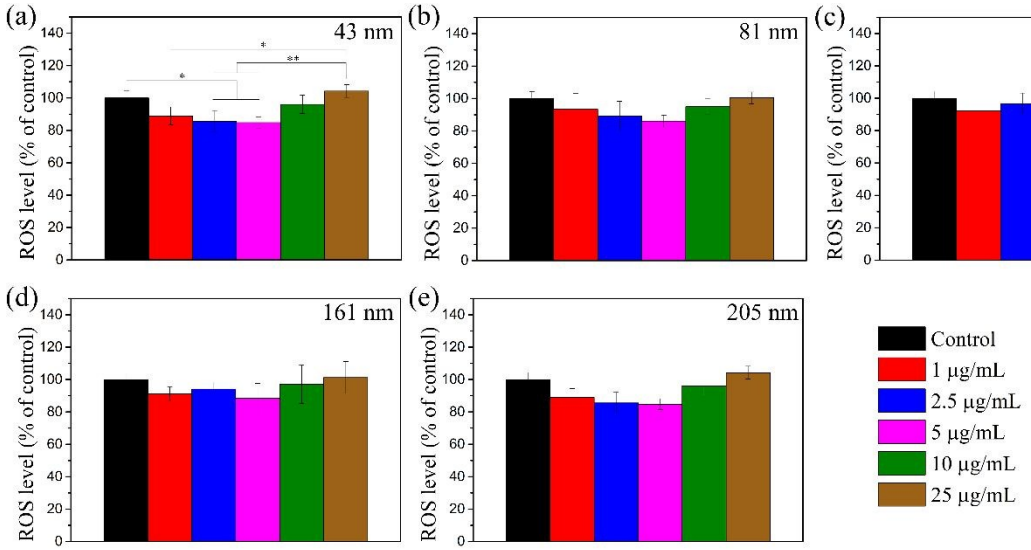

Fig. 8 ROS production of HDFs with different concentrations and sizes of Se NPs. A One-Way ANOVA followed by a Tukey's Post Hoc Test was used to compare means of experimental groups to that of the negative control group, * p-value < 0.05 and ** p-value < 0.01.

Discussion

Size effects of Se NPs on their antibacterial activity

Size is a key parameter that governs the antimicrobial activity of nanoparticles. For many nanoparticle systems, smaller particle size correlates with a stronger antimicrobial effect. For example, multiple studies have reported that smaller sizes of ZnO NPs [61, 62], Ag NPs [63-66], CuO NPs [67] and Au NPs [68] have a better antibacterial performance compared to larger particles of the same composition. However, some nanoparticle systems show improved antimicrobial activity when the particles are larger. For instance, Adams *et al.* investigated the antibacterial activity of Pd NPs with sizes of 2, 2.5 and 3.1 nm. The results demonstrated that the mid-sized (2.5 nm) Pd NPs were the most toxic to *S. aureus* [69]. Furthermore, Liu *et al.* investigated the size-dependent antibacterial activity of graphene oxide (GO) sheets and found that larger GO sheets had stronger antibacterial activity [70].

For Se NPs, the relationship between particle size and antimicrobial activity has not been previously elucidated. Although Zonaro *et al.* reported that smaller sized Se NPs exhibited higher antibacterial efficacy, the sizes of Se NPs they fabricated were relatively large, ranging from ~220 to ~360 nm [38].

This is the first systematic study that investigates how nanoparticle size impacts the antimicrobial efficacy of Se NPs, to our knowledge. The data presented herein clearly illustrates that the size of the Se NPs is a governing variable that controls their antimicrobial properties. Specifically, particles with a diameter of ~80 nm exhibit the most potent antimicrobial properties, as illustrated through both the growth inhibition and the CFU assays (Fig. 2-5 and Table 1).

Comparing the antibacterial activity of the 81 nm Se NPs fabricated here to previous reports, the 81 Se NPs showed outstanding antibacterial activity [27 28 31 71]. For example, Guisbiers *et al*. fabricated Se NPs of 115 ± 38 nm, and reported their MIC to *S. aureus* as 79 ± 4 μg/mL[27]. Tran *et al*. fabricated Se NPs with mean size of around 70 nm, and the MIC of these NPs to *S. aureus* was higher than 64 μg/mL [28]. In comparison, our 81 nm Se NPs have a significantly lower MIC of 16 ± 7 μg/mL. Although the 70 nm Se NPs fabricated by Tran *et al.* [28] were close to 81 nm Se NPs in terms of size, and also used PVA as stabilizer, their zeta potential was much more negative (-24 mV) than the 81 nm Se NPs fabricated here (-6.7 ± 4.5 mV), which may be ascribed to the different synthesis reagents used. As bacterial membranes are generally negatively charged [72], the more negatively charged NPs are less likely to approach bacteria and exert their antibacterial activity due to electrostatic repulsion between the NPs and the bacterial membranes [73, 74]. One study did produce Se NPs with an MIC as low as 4 μg/mL [75]. However, it is critical to point out that this was achieved by conjugating bactericidal compounds to the Se NP surfaces in order to boost their efficacy. As such, the particles produced in this work are the most potent Se NPs reported that do not rely on additional antimicrobial agents, according to the authors' knowledge.

Antibacterial mechanism of Se NPs

Antimicrobial NPs can damage bacterial cells through multiple pathways. It is this multimodal antimicrobial behaviour that makes these materials so appealing as it is expected to be more difficult for bacteria to develop resistance against the multiple forms of attack [6]. Various mechanisms of action have been illustrated for antimicrobial nanoparticles including: damaging the integrity of the bacterial cell membranes [76]; promoting ROS production that damages cellular components [77, 78], such as lipids, DNA and proteins; interrupting energy transduction by damaging mitochondrial components [56]; inactivating enzymes [79]; inhibiting DNA synthesis [76, 80]; and releasing metallic ions that exert toxicity towards the microbes [54, 56].

Although a number of papers have reported the antibacterial activity of Se NPs, the mechanism(s) by which they exert their antimicrobial effect has not been elucidated. Our data illustrates that the Se NPs do indeed negatively impact *S. aureus* through multiple mechanisms. Specifically, we observed that the all nanoparticles interfere with the metabolism of the bacteria through depletion of intracellular ATP, the 43 and 81 nm particles increased production of ROS and alter the

potential of the bacterial cell membrane, and that the 43 nm particles can cause membrane disruption.

ATP is the energy source used by cells to carry out many of their important biological processes, such as membrane transport, cell division, nodulation during nitrogen fixation, protein export, etc. [81] The depletion of ATP will likely affect these biological processes, resulting in loss of viability of the bacteria [54, 82, 83]. Membrane potential has important impacts on the spatial organisation of the cytoskeleton and cell division of the bacteria [84]. Disturbance of membrane potential can result in changes in various cellular processes related to bacterial viability [85]. In this study, Se NPs were found to deplete ATP and disrupt the potential of *S. aureus* membranes.

We observed that Se NPs promote ROS production in *S. aureus* cells, and oxidative stress induced by high ROS production is regarded as a very important mechanism of antibacterial activity [55]. For example, ROS can damage DNA, cell membranes, and cellular proteins to the point of cell death [77 86 87]; induce an increase in the concentration of cytosolic calcium [88]; result in the translocation of transcription factors [89]; and trigger the SOS response, a defence mechanism that halts the cell division process until DNA can be repaired [90].

Elemental selenium is not measurably soluble in aqueous environments [91, 92]. Therefore, the amount of Se ions released from Se NPs is likely to be very small. In this case, the effects of selenium ions on antibacterial activity may be too weak to be a significant antibacterial mechanism of Se NPs. However, the Se NPs can be transformed into organic forms in the bacteria [33], making them nutrients to the bacteria rather than damaging the cells. Many studies reported that Se NPs could be biotransferred to selenoproteins [93, 94]. The smaller Se NPs exhibited more active biotransformation than larger Se NPs [95]. In this study, the 43 nm Se NPs showed a lower ability than the 81nm ones to induce ROS production in *S. aureus* (Fig. 6(b)). This might be explained by the increased conversion of the smaller 43 nm Se NPs into selenoproteins by *S. aureus* cells. Approximately half of the characterized selenoproteins have antioxidant functions [96]. Although the 43 nm Se NPs promoted ROS production, production of selenoproteins from these Se NPs could potentially scavenge some of the produced ROS, reducing its harmful effects. Compared to 43 nm Se NPs, the 81 nm Se NPs may be more slowly converted into selenoproteins by *S. aureus* cells, resulting in less ROS scavenging ability. This would explain why the total ROS level in *S. aureus* cells treated with 43 nm Se NPs was lower than those treated with 81 nm NPs. The 124 nm Se NPs exhibited no significant effects on promotion of ROS production (Fig. 6(b)) and change of membrane potential (Fig. 6(c)) of *S. aureus* cells. These findings suggest that a balance must be achieved to generate the optimum antibacterial activity of Se NPs as a function of their size.

This study has identified multiple different modes by which the Se NPs may achieve their antimicrobial function. As such, these results will enable design of Se NP systems with improved antibacterial efficacy and underpin more detailed molecular biology experiments in the future to determine the exact molecular mechanisms of action.

Cytotoxicity of Se NPs

To develop new antimicrobial agents, their toxicity towards both the target organism and the host cells need to be investigated [32, 97]. In this work, HDFs treated with the highest tested concentration of Se NPs retained viabilities higher than 70%, indicating no cytotoxicity according to ISO 10993-5 [57]. Additionally, robust antimicrobial activity was observed at concentrations of 12.5 µg/mL. At comparable concentrations (10 µg/mL) the HDFs had the same viability (~100%) as the untreated controls. Furthermore, the viability assay was performed after 24 h of incubation of the nanoparticles with the HDFs compared to 90 min for the CFU assays on *S. aureus* and MRSA, illustrating their acute toxicity towards the bacteria and the benign interactions with the human cells at this concentration.

The cytotoxicity of NPs depends not only on the size, shape and surface chemistry of NPs, but also the tested cell line [98]. Human dermal fibroblasts have been considered as an appropriate cell line to test cytotoxicity of materials for dermatologic applications [99]. They have been used for cytotoxicity tests on many different types of NPs, such as Ag NPs[100], Au NPs[98], ZnO NPs [101], TiO_2 [102] and CeO_2 NPs [103]. However, cytotoxicity of Se NPs fabricated in this work on more specific cell types would also need to be further tested for potential applications of these Se NPs to specific areas of the human body.

Experimental

Materials

Selenium dioxide (SeO_2) and polyvinyl alcohol (PVA, MW 9000-10000, 80% hydrolysed) were purchased from Sigma Aldrich (Australia). Sodium thiosulphate ($Na_2S_2O_3$) was obtained from Science Supply Australia (Australia). Dimethyl sulfoxide (DMSO) was purchased from Fluka (Australia). Phosphate buffer solution (PBS) tablets were purchased from Gibco (UK). All water used was purified by Milli-Q water purification system (Merck Millipore, Massachusetts, USA).

Se NP synthesis

A reduction reaction was used to prepare the Se NPs. Selenium dioxide was used as the selenite precursor, sodium thiosulfate as the reducing agent, and PVA as the stabilizer. PVA was dissolved in Milli-Q water to a concentration of 10 mg/mL and SeO_2 was added to a final concentration of 5 mM. $Na_2S_2O_3$ was dissolved separately in Milli-Q water at a concentration of 20-600 mM, and 10 mL of this solution was added to the 10 mL of the PVA / SeO_2 solution under magnetic stirring conditions. The size of the Se NPs was controlled by varying the concentrations of reagents and the reaction times, as listed in Table S1. After the desired reaction time, the solution was aliquoted into 1 mL Eppendorf tubes and centrifuged at 13000 rpm (or 15500 g) for 10 min. The reaction solution was replaced with Milli-Q water to halt the reaction, and the Se NPs were redispersed using a vortex mixer. The above rinsing procedure was repeated once. After rinsing, the Se NPs were redispersed into PBS and stored at 4 °C until use. For biological tests, the Se NP suspensions were sterilized by filtering through 0.22 µm Millex-GV (PVDF) filters (Merck, Massachusetts, USA).

Se NP characterization

The size distributions and zeta potential of the Se NPs were measured using a Zetasizer (Malvern, ATA Scientific). Both measurements were performed at 25 °C. Selenium was selected as the material with a refractive index of 2.6 and an absorption of 0.5, and water was selected as the dispersant with refractive index of 1.330, a viscosity of 0.8872 cP and a dielectric constant of 78.5 [104].

The morphology and diffraction patterns of the Se NPs were assessed via transmission electron microscopy (TEM, TECNAI F20) using an accelerating voltage of 200 keV. Energy dispersive spectroscopy (EDS) was used to detect the component elements of the nanoparticles. The interaction between Se NPs and PVA was investigated by Fourier Transform Infrared Spectroscopy (FT-IR, Varian 7000).

To measure the total Se concentration of the Se NP suspensions, the particles were dissolved into ions through exposure to nitric acid, and inductively coupled plasma-optical emission spectrometry (ICP-OES, Varian 720-ES) was used to determine the Se ion concentrations.

The number concentrations of Se NPs were measured using a NanoSight NS 300 Instrument (Malvern Panalytical).

Antibacterial tests

To test the antibacterial activity of Se nanoparticles, bacterial growth inhibition assays and colony forming units (CFU) assays were performed. Groups with both the same weight concentration and the same number concentration of Se NPs were used for the growth inhibition test. The methods for determining the minimum inhibitory concentrations (MIC) and the minimum bactericidal concentrations (MBC) using a plate microdilution method are based on the CLSI 2015 guideline M07 and M26 [105], respectively and are detailed below.

The bacterial strains methicillin-sensitive *Staphylococcus aureus* (MSSA) ATCC 29213 and methicillin-resistant *Staphylococcus aureus* (MRSA) ATCC 43300 were obtained from the culture collection of The Melbourne Dental School, University of Melbourne, Australia. Bacteria were cultured in MHB at 37 °C. 100 µL of Se NPs in PBS with desired concentration of particles was added into each well of 96-well microplates. 100 µL MHB with 2.5×10^6 bacteria/mL was then added to the wells. 100 µL of the mixed solution was transferred into another microplate. For the growth inhibition test, one of the two microplates was put into an iEMS microplate reader (Pathtech Pty Ltd, Melbourne, Australia) controlled at 37 °C to monitor bacterial growth by measuring the absorbance at a wavelength of 630 nm for 24 h. Background absorbance values due to the Se NP solutions were subtracted from the measure absorbance values. For the CFU assay, the bacteria suspensions were incubated with Se NPs in the second microplate for 90 min at 37 °C. The bacterial suspensions were diluted to 10^{-1}, 10^{-2}, 10^{-3} and 10^{-4} times in PBS,10 µL of the solutions was transferred to agar plates with MHB, the agar plates were incubated overnight at 37 °C, and the bacterial colony forming units were observed and counted.

To calculate the Minimum Inhibitory Concentration (MIC), the absorbance values of bacteria growth curves at the time point when the stationary phase starts (t_{sps}) were taken and calculated as percentage of the untreated control ($Z=OD_a/OD_b\times100\%$, OD_a represents absorbance at t_{sps} of experimental groups and OD_b represents the absorbance at t_{sps} of the negative control group, all absorbance values are subtracted from the culture medium background values). Then concentration-inhibition curves were plotted with the percentages of absorbance, and linear regression analysis was adopted to determine the MIC at which Z becomes zero (Fig. S4).

To calculate the Minimum Bactericidal Concentration (MBC), concentration-killing curves were plotted with CFUs/mL as a function of antibacterial agent concentration, and linear regression analysis was used to determine the lowest concentration (MBC) at which the CFU/mL becomes zero (Fig. S5).

Adenosine triphosphate (ATP) tests

A 50 µL suspension containing the desired size and amount of Se NPs in PBS was added to each well of 96-well microplates. 50 µL of MHB with 2.5×10^6 bacteria/mL were also added to each well. After 1h of incubation at 37 °C, the 96-well microplates were transferred to room temperature for a further 30 min. 100 µL of BacTiter-Glo™ reagent (Promega, Australia) was added to each well, mixed on an orbital shaker, and incubated at room temperature for 5min. The luminescence was recorded using a microplate reader (PerkinElmer 1420 Multilabel Counter VICTOR3). A standard curve was generated using 10-fold serial dilutions of ATP from 1 µM to 10 pM in 100 µL MHB, adding 100 µL of BacTiter-Glo™ reagent, mixing on an orbital shaker and incubating for 1 min prior to measurement of luminescence.

ROS production tests

50 µL of a PBS suspension containing the desired concentration and size of Se NPs was added to each well of 96-well microplate. 50 µL of MHB with 2.5×10^6 cells/mL bacteria were added to each well. After 90 min incubation at 37 °C, CellROX® Orange Reagent was added into each well to a final concentration of 750 nM. The cells were incubated for an additional 1 h. The fluorescence from the CellROX Orange Reagent was measured on FL-3 using a Cell Lab Quanta SC MPL flow cytometer (Beckman Coulter). Two independent experiments were done for this test, and two technical replicates were performed for each independent experiment.

Membrane potential tests

Membrane potential change was measured using BacLight Bacterial Membrane Potential Kit (Invitrogen). *Staphylococcus aureus* were cultured in MHB at 37 °C. 50 µL of different concentrations and sizes of Se NPs in PBS solution was added into each well of 96-well microplates. Then 50 µL MHB with 2.5×10^6 cells/mL bacteria were added into each well. Adding 50 µL MHB with 2.5×10^6 cells/mL bacteria into 50 µL PBS acted as an untreated control. Adding carbonyl cyanide 3-chlorophenylhydrazone (CCCP) into the untreated control at a final concentration of 5 µM acted as a fully depolarized control. $DiOC_2(3)$ was added to all wells at a final concentration of 3mM. The $DiOC_2$ (3) dye exhibits green fluorescence in all bacterial cells when it is at low concentrations, but it becomes more concentrated in healthy bacteria cells which are maintaining their membrane potential, and the fluorescence shifts to be red. After 1h incubation at 37 °C, the membrane potential was determined using a Cell Lab Quanta SC MPL flow cytometer (Beckman Coulter) as the ratio of cells that exhibited red fluorescence (FL-3) to those that displayed green fluorescence (FL-1). Gates were drawn based on the untreated (polarized) and CCCP-treated (fully depolarized) controls. Two independent experiments were done for this test, and two technical replicates were adopted for each independent experiment.

Bacterial morphology imaging

Helium Ion Microscopy (HIM, Zeiss, Germany) was used to observe *Staphylococcus aureus* after treatment with Se NPs. The samples were prepared as follows: 100 µL of a 125 µg/mL suspension of Se NPs in PBS solution was added to each well of a 96-well microplate,

View Article Online
DOI: 10.1039/C9NR04421J

100 µL MHB with 1.25×10^7 cells/mL bacteria was added into each well. Samples were incubated for 90 min, 10 µL of the solution was pipetted on a clean silicon wafer, and allowed to air dry at 37 °C for 20 min. Samples were fixed using 2.5% glutaraldehyde for 1 h, and dehydrated in an ethanol gradient (30%, 50%, 60%, 70%, 80%, 90%, 95% and 100%) prior to imaging.

Cytotoxicity tests on human dermal fibroblasts

Human dermal fibroblasts (HDFs, obtained from Lonza, Australia) were cultured in the Dulbecco's modified Eagle's medium (DMEM) with 10% foetal bovine serum (FBS), 100 U·mL^{-1} penicillin and 100 µg·mL^{-1} streptomycin at 37 °C in a humidified atmosphere of 5% CO_2. Two methods were adopted to test the cytotoxicity of Se NPs towards HDFs, namely the Cell Counting Kit-8 (CCK-8) assay and lactate dehydrogenase (LDH) assay.

For the CCK-8 tests, filtered sterilised Se NPs suspensions were diluted in PBS to concentrations of 20, 50, 100, 200 and 500 µg/mL; 5% (v/v) of these diluted solutions were added to DMEM media to give final concentrations of Se NPs of 1, 2.5, 5, 10 and 25 µg/mL. Two control groups were used, pure DMEM as the negative control and DMEM with 10% (v/v) dimethyl sulfoxide (DMSO) as the positive control, according to ISO 10993-5 standard [57]. Cells were initially incubated in 96-well plates at a density of 4×10^3 cells per 100 µL DMEM per well and incubated for 24 h to allow attachment. The medium was then replaced by 100 µL of DMEM with Se NPs or control media. After 24 h incubation, the medium was removed, and the cultures were washed once with PBS. 120 µL of DMEM with 10% CCK-8 solution was added to each well and incubated for 3 h. Then, 100 µL medium was transferred from each well to new 96-well plates and the absorbance of each well at 450 nm was measured using a microplate reader (M200 PRO, Tecan). The cell viability (*X*) of each experimental group was calculated based on three samples according to formula 1.

$$X = \frac{OD_1}{OD_2} \times 100\% \quad (1)$$

OD_1 represents the mean absorbance of the experimental groups and the positive control group, and OD_2 represents the mean absorbance of the negative control group.

LDH is released from cells into the medium when cell lysis occurs. The amount of LDH released due to exposure to Se NPs was assessed as a measure of cytotoxicity using the Cyto Tox 96® nonradioactive assay (Promega, Madison, WI, USA) following the manufacturer's instructions. Briefly, the HDFs were cultured in a 96-well microplate for 24 h to allow attachment. The medium was aspirated and replaced with DMEM containing the desired concentrations of Se NPs and the cells were incubated for 6 h. The Cyto Tox 96 reagent was added to the wells, cultures were incubated for an additional 30 min, then the reaction was stopped by adding the stop solution. For the maximum LDH release control, HDFs were lysed using 1X lysis solution for 45 minutes before adding the Cyto Tox 96 reagent. A microplate reader (PerkinElmer 1420 Multilabel Counter VICTOR3) was used to measure the absorbance at 490 nm. The cytotoxicity (Y) was calculated according to formula 2:

$$Y = \frac{OD_3}{OD_4} \times 100\% \quad (2)$$

OD_3 represents the mean absorbance of experimental groups, and OD_4 represents the mean absorbance of the maximum LDH release control group. All absorbance values are after subtraction of the culture medium background values.

Measurements of reactive oxygen species (ROS) levels in HDF treated with Se NPs

The cells were seeded into 96-well plates at a density of 5×10^3 cells per 100 µL medium and incubated for 24 h to allow attachment. Se NP suspensions were diluted with PBS to concentrations of 20, 50, 100, 200 and 500 µg/mL, and 5% (v/v) of the diluted solution was added to DMEM to give the final concentrations of Se NPs in DMEM: 1, 2.5, 5, 10 and 25 µg/mL. DMEM with 5% PBS solution was used as the negative control. After 6 h of incubation, CellROX® Orange Reagent was added into each well to a final concentration of 5 µM. CellROX® Orange reagent is a membrane-permeable dye that does not fluoresce in its reduced state but does fluoresce when oxidized by ROS. The cells were incubated for 30 min with the CellROX® Orange reagent, the medium was removed, and the cells were washed three times with PBS. The fluorescence intensity of each well was tested with a plate reader (M200 PRO, Tecan) with an excitation wavelength of 545 nm and emission wavelength of 565 nm. The ROS production level was presented as a percentage of the control group. Three samples were tested for each group.

Statistical analysis

Data in this work are expressed as means ± standard deviation. Statistical analyses for all results were performed by one-way analysis of variance (ANOVA with Tukey's Post Hoc Test) using SPSS 22.0 software. p-values less than 0.05 were considered statistically significant.

Conclusions

In this work, amorphous and spherical Se NPs with sizes ranging from 43 to 205 nm were fabricated and their mammalian cytotoxicity and antibacterial activity were investigated. The antibacterial activity of Se NPs was size-dependent and dose-dependent. Se NPs with a mean size of 81 nm showed the highest efficacy on both growth inhibition and killing of *S. aureus* and MRSA. We additionally illustrated that the particles interact with the bacterial cells via multiple pathways that could lead to their antimicrobial properties, including disruption of energy transduction, increased ROS production, membrane depolarisation, and membrane disruption. No cytotoxic effect was observed towards HDFs over the range of concentrations studied. Additionally, the HDFs showed ~100% viability after exposure to 10 µg/mL of 81 nm Se NPs, a concentration that shows robust antimicrobial properties. Taking both the cytotoxicity and antibacterial activity test results into consideration, this work illustrates the highly effective antimicrobial properties of 81 nm Se NPs and supports further research in the development of Se NP antibacterial treatments.

Conflicts of interest

There are no conflicts to declare.

Acknowledgements

The authors thank Babak Nasr and the Materials Characterisation and Fabrication Platform (MCFP, the University of Melbourne) for help with HIM imaging. We would also like to thank the Bio21 Advanced Microscopy Facility (the University of Melbourne), the Particulate Fluids Processing Centre (PFPC) and the Oral Health CRC at the Melbourne Dental School for access to infrastructure and equipment. We thank Dr Phong A. Tran for useful discussions.

Notes and references

1. A. Prüss, D. Kay, L. Fewtrell and J. Bartram, *Environmental health perspectives*, 2002, **110**, 537-542.
2. M. J. Hajipour, K. M. Fromm, A. A. Ashkarran, D. J. de Aberasturi, I. R. de Larramendi, T. Rojo, V. Serpooshan, W. J. Parak and M. Mahmoudi, *Trends in biotechnology*, 2012, **30**, 499-511.
3. Y. Xie, Y. Liu, J. Yang, Y. Liu, F. Hu, K. Zhu and X. Jiang, *Angewandte Chemie International Edition*, 2018, **57**, 3958-3962.
4. A. J. Huh and Y. J. Kwon, *Journal of Controlled Release*, 2011, **156**, 128-145.
5. Q. Li, S. Mahendra, D. Y. Lyon, L. Brunet, M. V. Liga, D. Li and P. J. Alvarez, *Water research*, 2008, **42**, 4591-4602.
6. M. Mühling, A. Bradford, J. W. Readman, P. J. Somerfield and R. D. Handy, *Marine environmental research*, 2009, **68**, 278-283.
7. E. Weir, A. Lawlor, A. Whelan and F. Regan, *Analyst*, 2008, **133**, 835-845.
8. P. AshaRani, G. Low Kah Mun, M. P. Hande and S. Valiyaveettil, *ACS nano*, 2008, **3**, 279-290.
9. P. A. Tran, D. M. Hocking and A. J. O'Connor, *Materials Science and Engineering: C*, 2015, **47**, 63-69.
10. P. L. Drake and K. J. Hazelwood, *Annals of Occupational Hygiene*, 2005, **49**, 575-585.
11. E.-J. Park, E. Bae, J. Yi, Y. Kim, K. Choi, S. H. Lee, J. Yoon, B. C. Lee and K. Park, *Environmental toxicology and pharmacology*, 2010, **30**, 162-168.
12. M. Trop, M. Novak, S. Rodl, B. Hellbom, W. Kroell and W. Goessler, *Journal of Trauma and Acute Care Surgery*, 2006, **60**, 648-652.
13. E. Underwood, *Trace elements in human and animal nutrition*, Elsevier, 2012.
14. S. R. Mahmoodi, M. Bayati, S. H. Rad, E. K. Heidari, A. Foroumadi and K. Gilani, *Journal of Materials Science: Materials in Electronics*, 2013, **24**, 4554-4559.
15. N. Kumar, R. Kumar, S. Kumar and S. Chakarvarti, *Journal of Materials Science: Materials in Electronics*, 2014, **25**, 3537-3542.
16. G. Xi, K. Xiong, Q. Zhao, R. Zhang, H. Zhang and Y. Qian, *Crystal growth & design*, 2006, **6**, 577-582.
17. S. N. Barnaby, S. H. Frayne, K. R. Fath and I. A. Banerjee, *Soft Materials*, 2011, **9**, 313-334.
18. H. Zeng and G. F. Combs, *The Journal of nutritional biochemistry*, 2008, **19**, 1-7.
19. K. H. Lee and D. Jeong, *Mol Med Rep*, 2012, **5**, 299-304.
20. X. Zhai, C. Zhang, G. Zhao, S. Stoll, F. Ren and X. Leng, *Journal of Nanobiotechnology*, 2017, **15**, 4.
21. A. J. Kora, *IET nanobiotechnology*, 2018, **12**, 658-662.
22. I. Benko, G. Nagy, B. Tanczos, E. Ungvari, A. Sztrik, P. Eszenyi, J. Prokisch and G. Banfalvi, *Environmental Toxicology and Chemistry*, 2012, **31**, 2812-2820.
23. C. Hu, Y. Li, L. Xiong, H. Zhang, J. Song and M. Xia, *Animal feed science and technology*, 2012, **177**, 204-210.
24. L. Shi, W. Xun, W. Yue, C. Zhang, Y. Ren, L. Shi, Q. Wang, R. Yang and F. Lei, *Small Ruminant Research*, 2011, **96**, 49-52.
25. J. Zhang and J. E. Spallholz, *General, Applied and Systems Toxicology*, 2011.
26. A. Ionin, A. Ivanova, R. Khmel'nitskii, Y. V. Klevkov, S. Kudryashov, A. Levchenko, A. Nastulyavichus, A. Rudenko, I. Saraeva and N. Smirnov, *Laser Physics Letters*, 2017, **15**, 015604.
27. G. Guisbiers, Q. Wang, E. Khachatryan, L. Mimun, R. Mendoza-Cruz, P. Larese-Casanova, T. Webster and K. Nash, *International journal of nanomedicine*, 2016, **11**, 3731.
28. P. A. Tran, N. O'Brien-Simpson, E. C. Reynolds, N. Pantarat, D. P. Biswas and A. J. O'Connor, *Nanotechnology*, 2015, **27**, 045101.
29. P. A. Tran and T. J. Webster, *Int J Nanomedicine*, 2011, **6**, 1553-1558.
30. S. Shoeibi and M. Mashreghi, *Journal of Trace Elements in Medicine and Biology*, 2017, **39**, 135-139.
31. E. Cremonini, M. Boaretti, I. Vandecandelaere, E. Zonaro, T. Coenye, M. M. Lleo, S. Lampis and G. Vallini, *Microbial Biotechnology*, 2018, **11**, 1037-1047.
32. D. P. Biswas, N. M. O'Brien-Simpson, E. C. Reynolds, A. J. O'Connor and P. A. Tran, *Journal of colloid and interface science*, 2018.
33. M. Palomo-Siguero, A. M. a. Gutiérrez, C. Pérez-Conde and Y. Madrid, *Microchemical Journal*, 2016, **126**, 488-495.
34. P. Sonkusre and S. S. Cameotra, *Colloids and Surfaces B: Biointerfaces*, 2015, **136**, 1051-1057.
35. M. Masae, P. Pitsuwan, K. Kooptarnond, P. Choopool, S. Kachintararot, J. Siriwan and A. Ficai, 2018.
36. A. Nastulyavichus, S. Kudryashov, N. Smirnov, I. Saraeva, A. Rudenko, E. Tolordava, A. Ionin, Y. Romanova and D. Zayarny, *Applied Surface Science*, 2019, **469**, 220-225.
37. O. Bilek, Z. Fohlerova and J. Hubalek, *PloS one*, 2019, **14**, e0214066.
38. E. Zonaro, S. Lampis, R. J. Turner, S. J. S. Qazi and G. Vallini, *Frontiers in microbiology*, 2015, **6**.
39. J. Yip, L. Liu, K. H. Wong, P. H. Leung, C. W. M. Yuen and M. C. Cheung, *Journal of Applied Polymer Science*, 2014, **131**.
40. A.-W. A. Ismail, N. M. Sidkey, R. A. Arafa, R. M. Fathy and A. I. El-Batal, *British Biotechnology Journal*, 2016, **12**, 1.
41. G. Guisbiers, H. H. Lara, R. Mendoza-Cruz, G. Naranjo, B. A. Vincent, X. G. Peralta and K. L. Nash, *Nanomedicine: Nanotechnology, Biology and Medicine*, 2016.
42. A. Albanese, P. S. Tang and W. C. Chan, *Annual review of biomedical engineering*, 2012, **14**, 1-16.
43. E. C. Cho, Q. Zhang and Y. Xia, *Nature nanotechnology*, 2011, **6**, 385.
44. A. Verma and F. Stellacci, *Small*, 2010, **6**, 12-21.
45. B. D. Chithrani, A. A. Ghazani and W. C. Chan, *Nano letters*, 2006, **6**, 662-668.

46. H. Ardani, C. Imawan, W. Handayani, D. Djuhana, A. Harmoko and V. Fauzia, 2017.
47. A. A. Becaro, C. M. Jonsson, F. C. Puti, M. C. Siqueira, L. H. Mattoso, D. S. Correa and M. D. Ferreira, *Environmental Nanotechnology, Monitoring & Management*, 2015, **3**, 22-29.
48. J. Zhang, H. Wang, Y. Bao and L. Zhang, *Life sciences*, 2004, **75**, 237-244.
49. S.-Y. Lin, W.-T. Cheng, Y.-S. Wei and H.-L. Lin, *Polymer journal*, 2011, **43**, 577.
50. Z. Mbhele, M. Salemane, C. Van Sittert, J. Nedeljković, V. Djoković and A. Luyt, *Chemistry of Materials*, 2003, **15**, 5019-5024.
51. B. Yu, Y. Zhang, W. Zheng, C. Fan and T. Chen, *Inorganic chemistry*, 2012, **51**, 8956-8963.
52. B. Nandini, P. Hariprasad, H. S. Prakash, H. S. Shetty and N. Geetha, *Scientific Reports*, 2017, **7**.
53. R. Mempin, H. Tran, C. Chen, H. Gong, K. K. Ho and S. Lu, *BMC microbiology*, 2013, **13**, 301.
54. C.-N. Lok, C.-M. Ho, R. Chen, Q.-Y. He, W.-Y. Yu, H. Sun, P. K.-H. Tam, J.-F. Chiu and C.-M. Che, *JBIC Journal of Biological Inorganic Chemistry*, 2007, **12**, 527-534.
55. Y. Li, W. Zhang, J. Niu and Y. Chen, *ACS nano*, 2012, **6**, 5164-5173.
56. C.-N. Lok, C.-M. Ho, R. Chen, Q.-Y. He, W.-Y. Yu, H. Sun, P. K.-H. Tam, J.-F. Chiu and C.-M. Che, *Journal of proteome research*, 2006, **5**, 916-924.
57. E. Iso, *Tests for in vitro cytotoxicity*, 2009.
58. S. Malhotra, M. Welling, S. Mantri and K. Desai, *Journal of Biomedical Materials Research Part B: Applied Biomaterials*, 2016, **104**, 993-1003.
59. H.-h. WANG and Z.-c. XIE, *Acta Zoonutrimenta Sinica*, 2003, **3**, 001.
60. T. Chen, Y.-S. Wong, W. Zheng, Y. Bai and L. Huang, *Colloids and surfaces B: Biointerfaces*, 2008, **67**, 26-31.
61. K. R. Raghupathi, R. T. Koodali and A. C. Manna, *Langmuir*, 2011, **27**, 4020-4028.
62. O. Yamamoto, *International Journal of Inorganic Materials*, 2001, **3**, 643-646.
63. S. Agnihotri, S. Mukherji and S. Mukherji, *Rsc Advances*, 2014, **4**, 3974-3983.
64. Z. Lu, K. Rong, J. Li, H. Yang and R. Chen, *Journal of materials science: Materials in medicine*, 2013, **24**, 1465-1471.
65. M. A. Raza, Z. Kanwal, A. Rauf, A. N. Sabri, S. Riaz and S. Naseem, *Nanomaterials*, 2016, **6**, 74.
66. A. Ivask, I. Kurvet, K. Kasemets, I. Blinova, V. Aruoja, S. Suppi, H. Vija, A. Käkinen, T. Titma and M. Heinlaan, *PloS one*, 2014, **9**, e102108.
67. A. Azam, A. S. Ahmed, M. Oves, M. Khan and A. Memic, *International Journal of Nanomedicine*, 2012, **7**, 3527.
68. S. Mihai and M. Malaisteanu, *Rev Chim Bucharest*, 2013, **64**, 105-107.
69. C. P. Adams, K. A. Walker, S. O. Obare and K. M. Docherty, *PLoS One*, 2014, **9**, e85981.
70. S. Liu, M. Hu, T. H. Zeng, R. Wu, R. Jiang, J. Wei, L. Wang, J. Kong and Y. Chen, *Langmuir*, 2012, **28**, 12364-12372.
71. M. Shakibaie, H. Forootanfar, Y. Golkari, T. Mohammadi-Khorsand and M. R. Shakibaie, *Journal of Trace Elements in Medicine and Biology*, 2015, **29**, 235-241.
72. Y.-C. Chung, Y. P. Su, C.-C. Chen, G. Jia, H. L. Wang, J. G. Wu and J. G. Lin, *Acta pharmacologica sinica*, 2004, **25**, 932-936.
73. P. K. Stoimenov, R. L. Klinger, G. L. Marchin and K. J. Klabunde, *Langmuir*, 2002, **18**, 6679-6686.
74. T. Hamouda and J. Baker Jr, *Journal of applied microbiology*, 2000, **89**, 397-403.
75. X. Huang, X. Chen, Q. Chen, Q. Yu, D. Sun and J. Liu, *Acta biomaterialia*, 2016, **30**, 397-407.
76. L. Wang, C. Hu and L. Shao, *International journal of nanomedicine*, 2017, **12**, 1227.
77. G. Applerot, A. Lipovsky, R. Dror, N. Perkas, Y. Nitzan, R. Lubart and A. Gedanken, *Advanced Functional Materials*, 2009, **19**, 842-852.
78. G. Tong, F. Du, W. Wu, R. Wu, F. Liu and Y. Liang, *Journal of Materials Chemistry B*, 2013, **1**, 2647-2657.
79. Y. N. Slavin, J. Asnis, U. O. Häfeli and H. Bach, *Journal of nanobiotechnology*, 2017, **15**, 65.
80. E. Hoseinzadeh, P. Makhdoumi, P. Taha, H. Hossini, J. Stelling and M. Amjad Kamal, *Current drug metabolism*, 2017, **18**, 120-128.
81. C. F. Higgins, I. D. Hiles, G. P. Salmond, D. R. Gill, J. A. Downie, I. J. Evans, I. B. Holland, L. Gray, S. D. Buckel and A. W. Bell, *Nature*, 1986, **323**, 448.
82. Y. Chen and T. Montville, *Journal of applied bacteriology*, 1995, **79**, 684-690.
83. S. Ennahar, K. Sonomoto and A. Ishizaki, *Journal of Bioscience and Bioengineering*, 1999, **87**, 705-716.
84. H. Strahl and L. W. Hamoen, *Proceedings of the National Academy of Sciences*, 2010, **107**, 12281-12286.
85. P. L. Páez, M. C. Becerra and I. Albesa, *BioMed research international*, 2013, **2013**.
86. K. Pulskamp, S. Diabaté and H. F. Krug, *Toxicology letters*, 2007, **168**, 58-74.
87. D. Chudobova, K. Cihalova, S. Dostalova, B. Ruttkay-Nedecky, M. A. Merlos Rodrigo, K. Tmejova, P. Kopel, L. Nejdl, J. Kudr and J. Gumulec, *FEMS microbiology letters*, 2014, **351**, 195-201.
88. D. Brown, K. Donaldson, P. Borm, R. Schins, M. Dehnhardt, P. Gilmour, L. Jimenez and V. Stone, *American Journal of Physiology-Lung Cellular and Molecular Physiology*, 2004, **286**, L344-L353.
89. V. Castranova, *Free radical biology and medicine*, 2004, **37**, 916-925.
90. J. STAVANS, in *Dynamics of Complex Interconnected Systems: Networks and Bioprocesses*, Springer, 2006, pp. 39-47.
91. D. Maiers, P. Wichlacz, D. Thompson and D. Bruhn, *Appl. Environ. Microbiol.*, 1988, **54**, 2591-2593.
92. S. Skalickova, V. Milosavljevic, K. Cihalova, P. Horky, L. Richtera and V. Adam, *Nutrition*, 2017, **33**, 83-90.
93. S. Sadeghian, G. A. Kojouri and A. Mohebbi, *Biological trace element research*, 2012, **146**, 302-308.
94. M. A. Rezvanfar, M. A. Rezvanfar, A. R. Shahverdi, A. Ahmadi, M. Baeeri, A. Mohammadirad and M. Abdollahi, *Toxicology and applied pharmacology*, 2013, **266**, 356-365.
95. Y. Wang, P. Chen, G. Zhao, K. Sun, D. Li, X. Wan and J. Zhang, *Food and Chemical Toxicology*, 2015, **85**, 71-77.
96. H. Tapiero, D. Townsend and K. Tew, *Biomedicine & pharmacotherapy*, 2003, **57**, 134-144.
97. S. J. Lam, N. M. O'Brien-Simpson, N. Pantarat, A. Sulistio, E.

View Article Online
DOI: 10.1039/C9NR04424H

H. Wong, Y.-Y. Chen, J. C. Lenzo, J. A. Holden, A. Blencowe and E. C. Reynolds, *Nature Microbiology*, 2016, **1**, 16162.

98. D. Mateo, P. Morales, A. Ávalos and A. I. Haza, *Journal of Experimental Nanoscience*, 2015, **10**, 1401-1417.
99. E. Hidalgo, R. Bartolomé, C. Barroso, A. Moreno and C. Domínguez, *Skin Pharmacology and Physiology*, 1998, **11**, 140-151.
100. A. Avalos, A. I. Haza, D. Mateo and P. Morales, *International wound journal*, 2016, **13**, 101-109.
101. K. Meyer, P. Rajanahalli, M. Ahamed, J. J. Rowe and Y. Hong, *Toxicology in vitro*, 2011, **25**, 1721-1726.
102. Z. Pan, W. Lee, L. Slutsky, R. A. Clark, N. Pernodet and M. H. Rafailovich, *Small*, 2009, **5**, 511-520.
103. L. Benameur, M. Auffan, M. Cassien, W. Liu, M. Culcasi, H. Rahmouni, P. Stocker, V. Tassistro, J.-Y. Bottero and J. m. Rose, *Nanotoxicology*, 2015, **9**, 696-705.
104. H. Hinterwirth, S. K. Wiedmer, M. Moilanen, A. Lehner, G. Allmaier, T. Waitz, W. Lindner and M. Lämmerhofer, *Journal of separation science*, 2013, **36**, 2952-2961.
105. CLSI, *Wayne, PA: Clinical and Laboratory Standards Institute*, 2015.